REVERSE TIME MIGRATION OF TTI MEDIA USING THE DECOMPOSED WAVEFIELD

LIWEI SONG, YING SHI* and XUAN KE

Northeast Petroleum University, Daqing Heilongjiang 163318, P.R. China.
* zhidao90@163.com

ABSTRACT

Song, L.W., Shi, Y. and Ke, X., 2019. Reverse time migration of TTI media using the decomposed wavefield. *Journal of Seismic Exploration*, 28: 245-256.

Reverse time migration (RTM) produces complex structure imaging with full wavefield information. This is the highest-precision imaging method to date. Compared with isotropic media RTM, imaging accuracy is assured by adding anisotropic constraints to seismic wavefields. Because of the sharp changes of velocity in the model, seismic wavefields generate strong reflection energy which causes noise or even false structure in the migration results. The main controlling factors of the anisotropic parameters were analyzed in this study by numerical simulation. The Hilbert transform was used to decompose the full wavefields in tilted transversely isotropic (TTI) media. The migration results were produced by cross-correlation of the decomposed wavefield imaging condition. Numerical examples show that the method obtains imaging results with high signal-to-noise ratio in TTI media.

INTRODUCTION

Whitemore (1983) proposed a reverse time migration (RTM) method based on the two-way wave equation, which could be used for imaging with full wavefields for reflection, refraction and multiple waves. RTM is not affected by changes of media velocity, so it is the first choice when dealing with complex structural imaging. Based on RTM, a series of methods for improving inversion accuracy were developed, such as least-squares reverse time migration (Xuan, 2018) and full waveform inversion (Xubao, 2017).

The present study showed that the anisotropy of seismic waves is often caused by thin interbeds of either sandy shale or limestone shale, or by vertical cracks in large rocks (Thomsen, 1986). When the crack size and spacing are less than the seismic wavelength, wave propagation can also be described in terms of the equivalent anisotropic media. In order to achieve high-precision imaging of complex media, it is necessary to increase the anisotropic constraints of the seismic wavefield.

Alkhalifah (1998) proposed the famous acoustic approximation idea on the basis of the dispersion relationship, and derived the fourth-order quasi-P (qP) wave equation in vertical transversely isotropic (VTI) media. Because the equation has the same frequency dispersion relation as the elastic wave equation, the characteristics of the qP wavefield are the same. Although zero shear-wave velocity is assumed along the axis, false quasi-SV (qSV) waves are still present in the wavefields. Zhou (2006) introduced auxiliary variables to simplify the qP-wave equation from fourth-order to second-order to achieve computationally efficient qP-wave numerical simulation. A new stable wave equation has been derived from Hooke's law and acoustic approximation (Duveneck et al., 2011; Zhang et al., 2011) in which the energy remains stable during the numerical simulation process. Fletcher (2009) derived a tilted transversely isotropic (TTI) media wave equation by coordinate transformation and obtained the RTM by introducing a stability factor into the coupled qP-wave equation, which enhances its adaptability to complex structures.

Another way of eliminating false qSV waves is to set the unstable region of the model to elliptical anisotropy, but change the local characteristics of the model (Yoon et al., 2010). In order to solve the disturbance of false qSV wave in essence, the rapid expansion method (Pestana et al., 2010, 2011) is applied to the numerical simulation of a seismic wavefield. This leads to a certain approximation when dealing with complex TI media. Xu (2014) derived a pure qP-wave equation with accurate kinematic characteristics, suitable for complex VTI models.

Cross-correlation imaging is often used in RTM since it avoids the problem of numerical instability caused by the calculation of reflection coefficients, but the result includes low-frequency noise. Liu (2010) proposed a filtering method to effectively suppress low-frequency noise in the wave number domain. Considering the spatial location relationship of the observation system, Yoon (2006) made use of the Poynting vector to improve the image quality. Fei (2015) obtained the up-going and down-going wavefields by decomposing full seismic wavefields, then screening the required wavefields to image (e.g., the down-going source wavefield and the up-going receiver wavefield). This method is effective but it needs to save all the wavefield data at each time step, so the calculation efficiency is very low. Shen (2015) proposed a seismic wavefield decomposition method based on the Hilbert transform, which reduces computer storage requirements.

In the present study, the seismic wavefield of TTI media was obtained by using the pure qP-wave equation, studying the main factors that determine the Thomsen parameters, and analyzing the noise-generation principle of RTM imaging results. The RTM results for the TTI media model were obtained by cross-correlating the imaging condition of the decomposed seismic wavefields. The numerical results show that the proposed method effectively suppresses noise and false images.

THEORY

Finite difference scheme for pure qP-wave equation

Early TTI media for RTM used the coupled qP-wave equation. Due to the difference in auxiliary functions, the wave equation form differs slightly. Considering such factors as the amount of calculation, computer storage, qSV-wavefield interference and wavefield stability, Xu (2014) proposed using the pure qP-wave equation to study seismic wavefield characteristics in VTI media. On this basis, the pure qP-wave equation of the TTI media is

$$\frac{\partial^2 u}{\partial t^2} = \frac{v^2}{2}\left[1 + 2\varepsilon\,\tilde{n}_x^2 + \sqrt{[(1+2\varepsilon)\,\tilde{n}_x^2 + \tilde{n}_z^2]^2 - 8(\varepsilon-\delta)\,\tilde{n}_x^2\,\tilde{n}_z^2}\right]\left(\frac{\partial^2 u}{\partial \tilde{x}^2} + \frac{\partial^2 u}{\partial \tilde{z}^2}\right), \quad (1)$$

where v is the phase velocity of the qP wave along the axis of symmetry; u is the wave field; ε and δ are the Thomsen parameters; $\tilde{N} = (\tilde{n}_x, \tilde{n}_z)$ is the rotated unit vector; and $(\tilde{x}, \tilde{z})$ is the rotated space coordinate, in which the symbol $\sim$ is the rotation operator. Applying the rotation matrix, we obtain the spatial differential:

$$\frac{\partial^2}{\partial \tilde{x}^2} = \sin^2\theta\frac{\partial^2}{\partial z^2} + \cos^2\theta\frac{\partial^2}{\partial x^2} + \sin 2\theta\frac{\partial^2}{\partial x\partial z}$$
$$\frac{\partial^2}{\partial \tilde{z}^2} = \sin^2\theta\frac{\partial^2}{\partial x^2} + \cos^2\theta\frac{\partial^2}{\partial z^2} - \sin 2\theta\frac{\partial^2}{\partial x\partial z} \qquad , \qquad (2)$$

where θ is the dip angle; and $\tilde{N}$ is calculated from

$$\tilde{N} = (\tilde{n}_x, \tilde{n}_z) \approx \left(\frac{\partial u}{\partial \tilde{x}}, \frac{\partial u}{\partial \tilde{z}} \right) = \left(\frac{\partial u}{\partial x}\cos\theta + \frac{\partial u}{\partial z}\sin\theta, -\frac{\partial u}{\partial x}\sin\theta + \frac{\partial u}{\partial z}\cos\theta \right) . \quad (3)$$

Using the finite difference numerical method, eq. (1) takes the following form:

$$u^{k+1} = 2u^k - u^{k-1} +$$

$$\Delta t^2 \frac{v_0^2}{2} \left[1 + 2\varepsilon\, \tilde{n}_x^{k\,2} + \sqrt{[(1+2\varepsilon)\tilde{n}_x^{k\,2} + \tilde{n}_z^{k\,2}]^2 - 8(\varepsilon-\delta)\tilde{n}_x^{k\,2}\,\tilde{n}_z^{k\,2}} \right]$$

$$\left(\begin{array}{l} \cos^2\theta \sum_{n=1}^{N} a_n \left(u^k_{i+n,j} + u^k_{i-n,j} \right)/\Delta x^2 + \sin^2\theta \sum_{m=1}^{M} b_m \left(u^k_{i,j+m} + u^k_{i,j-m} \right)/\Delta z^2 - \\ \sin 2\theta \sum_{n=1}^{N} c_n \sum_{m=1}^{M} d_m \left(u^k_{i+n,j+m} - u^k_{i+n,j-m} - u^k_{i-n,j+m} + u^k_{i-n,j-m} \right)/(\Delta x \Delta z) + \\ \sin^2\theta \sum_{n=1}^{N} a_n \left(u^k_{i+n,j} + u^k_{i-n,j} \right)/\Delta x^2 + \cos^2\theta \sum_{m=1}^{M} b_m \left(u^k_{i,j+m} + u^k_{i,j-m} \right)/\Delta z^2 + \\ \sin 2\theta \sum_{n=1}^{N} c_n \sum_{m=1}^{M} d_m \left(u^k_{i+n,j+m} - u^k_{i+n,j-m} - u^k_{i-n,j+m} + u^k_{i-n,j-m} \right)/(\Delta x \Delta z) \end{array} \right)$$

$$(4)$$

where k is the time step, and a_n, b_m, c_n and d_m are the finite difference coefficients.

Imaging condition

The cross-correlation imaging condition is represented by

$$I(x,z) = \int_0^{t_{max}} S(x,z,t) R(x,z,t_{max}-t)\, dt , \quad (5)$$

where $I(x,z)$ is the image; $S(x,z,t)$ is the source wavefield; $R(x,z,t_{max}-t)$ is the receiver wavefield; and t_{max} is the maximum seismic recording time.

Because the two-way wave equation is used, the source wavefield has up-going S_u and down-going S_d. Similarly, the receiver wavefield has up-going R_u and down-going R_d. Then eq. (5) takes the form

$$I(x,z) = \int_0^{t_{max}} (S_u + S_d)(R_u + R_d)dt = \int_0^{t_{max}} S_u R_u dt + \int_0^{t_{max}} S_u R_d dt + \int_0^{t_{max}} S_d R_u dt + \int_0^{t_{max}} S_d R_d dt .$$

(6)

When the full wavefield imaging gives four cross-correlation results, it is well established that $\int S_u R_u dt$ and $\int S_d R_d dt$ lead to low-frequency noise in the full wavefield cross-correlation images. The physical meaning of the other two terms are shown in Fig. 1, in which the solid ray is the true image for RTM, and the dashed line indicates a false image. Therefore, the equation for imaging conditions should be

$$I(x,z) = \int_0^{t_{max}} S_d R_u dt .$$

(7)
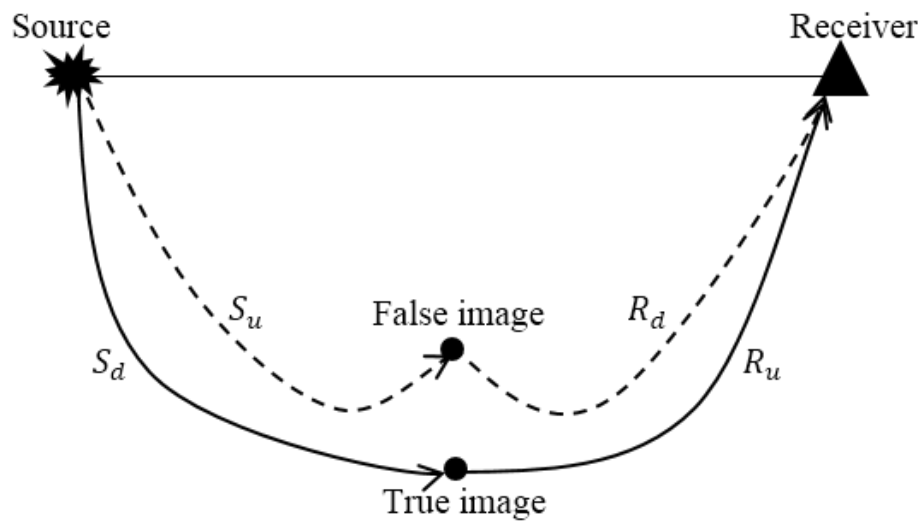
Fig. 1. Solid ray creates true image, dashed ray creates false image. S_u is up-going source wavefield, S_d is down-going source wavefield, R_u is up-going receiver wavefield, and R_d is down-going receiver wavefield

The seismic wavefield decomposition obtained by eq. (8), proposed by Shen (2015):

$$S_d(x,z,t) = \frac{1}{2}(1 + H_z H_t)S(z,t)$$

$$S_u(x,z,t) = \frac{1}{2}(1 - H_z H_t)S(z,t)$$

$$R_d(x,z,t) = \frac{1}{2}(1 + H_z H_t)R(z,t)$$ \hfill (8)

$$R_u(x,z,t) = \frac{1}{2}(1 - H_z H_t)R(z,t)$$

where H_z is the Hilbert transform operator in the vertical direction, and H_t is the Hilbert transform operator in the time direction.

EXAMPLES

Pure qP-wavefield simulation base by finite difference method

For TTI media, the kinematic properties of the qP wavefield depend on the velocity along the axis of symmetry, the symmetry axis angle θ, and the Thomsen parameters ε and δ. The physical meaning of each parameter was studied by simulation. In the homogeneous TTI media test models, the distance between grids was 10 m and the velocity was 3000 m/s. The source wavelet for these examples was a Ricker wavelet of 20 Hz dominant frequency; time sampling rate was 1 ms. Snapshots of the seismic wavefield are shown in Fig. 2.

The wave front is a circle in Fig. 2a due to equal velocities in all directions, equivalent to the seismic wavefield in an isotropic medium. Figs. 2b, 2c show that the seismic wavefield propagation velocity is least in the vertical direction and greatest in the horizontal direction. The two dashed lines in Figs. 2d, 2e show the fastest seismic wavefield propagation. As the Thomsen parameters ε and δ increase, the anisotropic characteristics are more obvious; the wavefield is determined by ε and δ in Fig. 2f. The wavefield snapshot for a non-zero angle of symmetry axis is shown in Fig. 2g.

Up-going and down-going wave decomposition in TTI media

A graben model was designed to verify the effect of seismic wavefield decomposition in TTI media. The model parameters are shown in Figs. 3a-d. The source was located in the center of the model. Fig. 4a shows the source wavefield snapshot at 600 ms, which contains information of the up-going and down-going wavefields. Due to the constraints of the anisotropic parameters, the wavefield snapshot does not exhibit spatial symmetry. The seismic wavefields based on eq. (8) decomposition are shown in Figs. 3b and 3c. Numerical experiments show that the Hilbert transform effectively decomposed the seismic wavefields in TTI media.
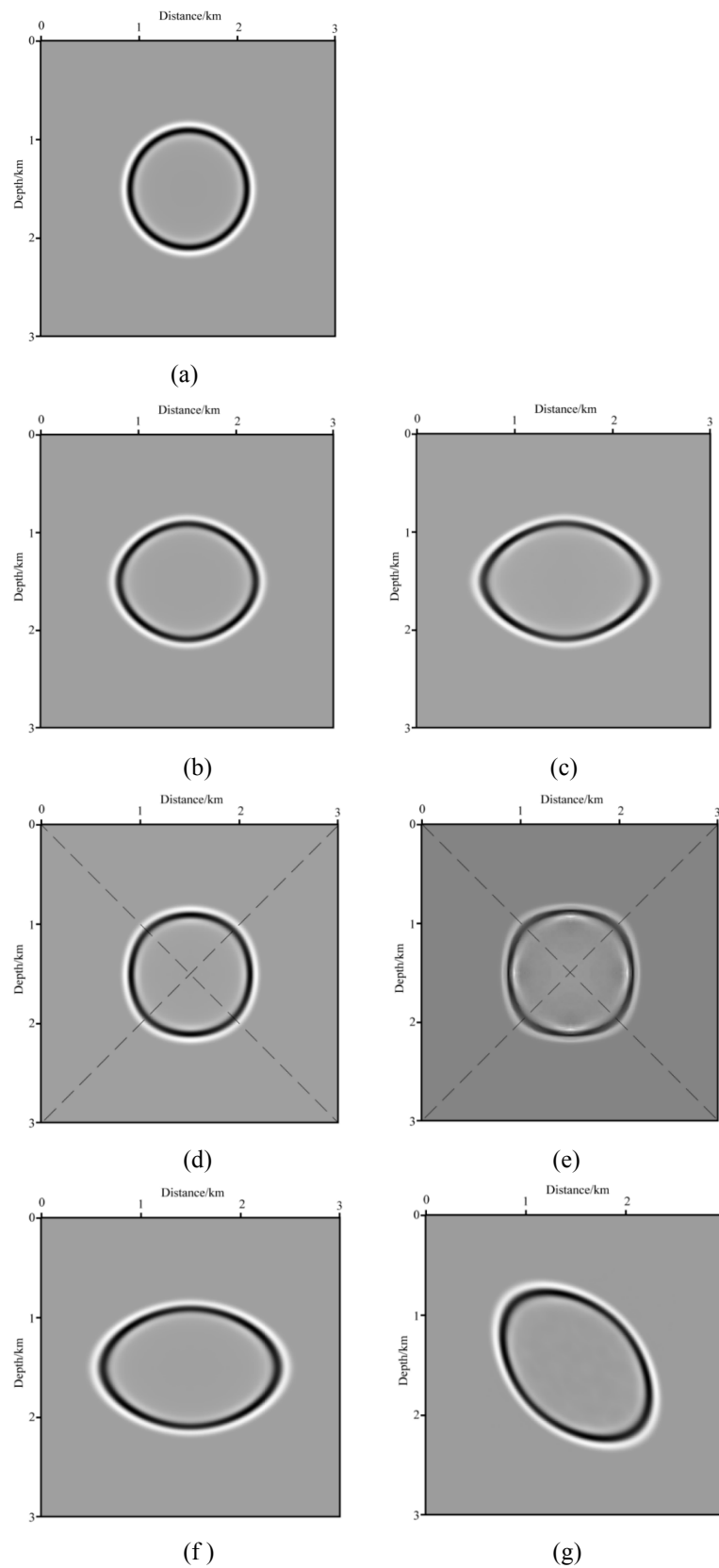
Fig. 2. Wavefield snapshots at 300 ms for parameters.

(a) $\theta = 0^o, \delta = 0, \varepsilon = 0$; (b) $\theta = 0^o, \delta = 0, \varepsilon = 0.2$; (c) $\theta = 0^o, \delta = 0, \varepsilon = 0.5$; (d) $\theta = 0^o, \delta = 0.2, \varepsilon = 0$;
(e) $\theta = 0^o, \delta = 0.5, \varepsilon = 0$; (f) $\theta = 0^o, \delta = 0.2, \varepsilon = 0.5$; (g) $\theta = 45^o, \delta = 0.2, \varepsilon = 0.5$
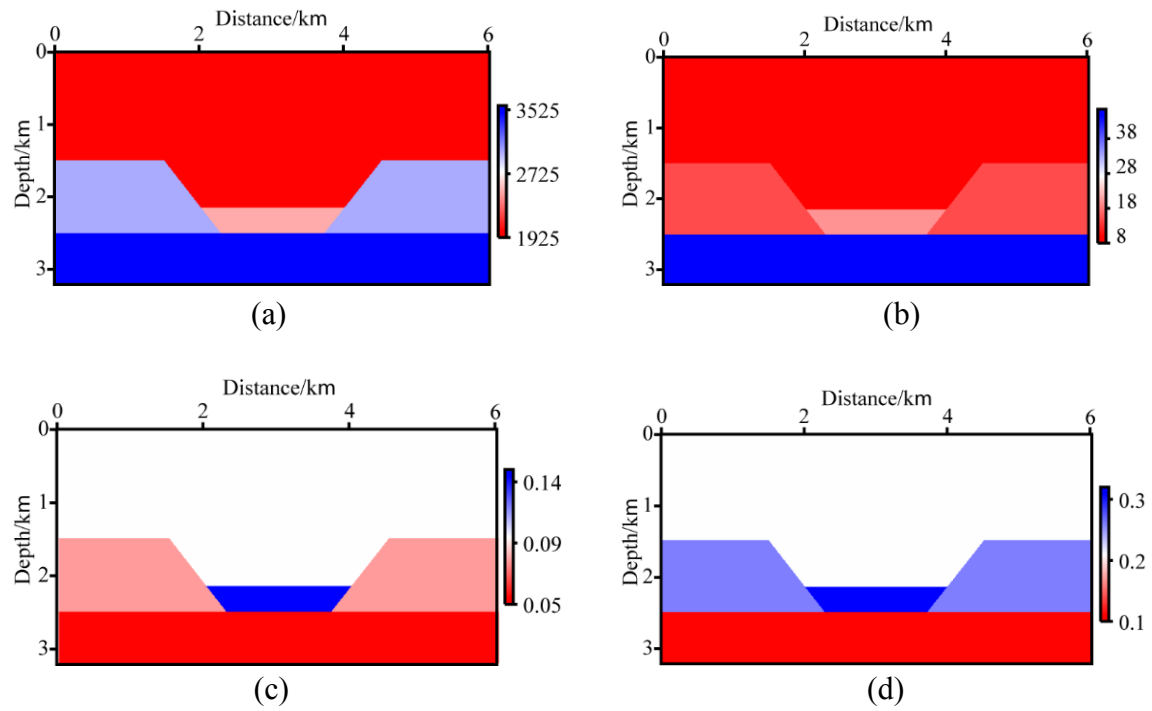
Fig. 3. TTI media model. (a) qP wave velocity along symmetry axis; (b) angle of symmetry axis; (c) ε; (d) δ.
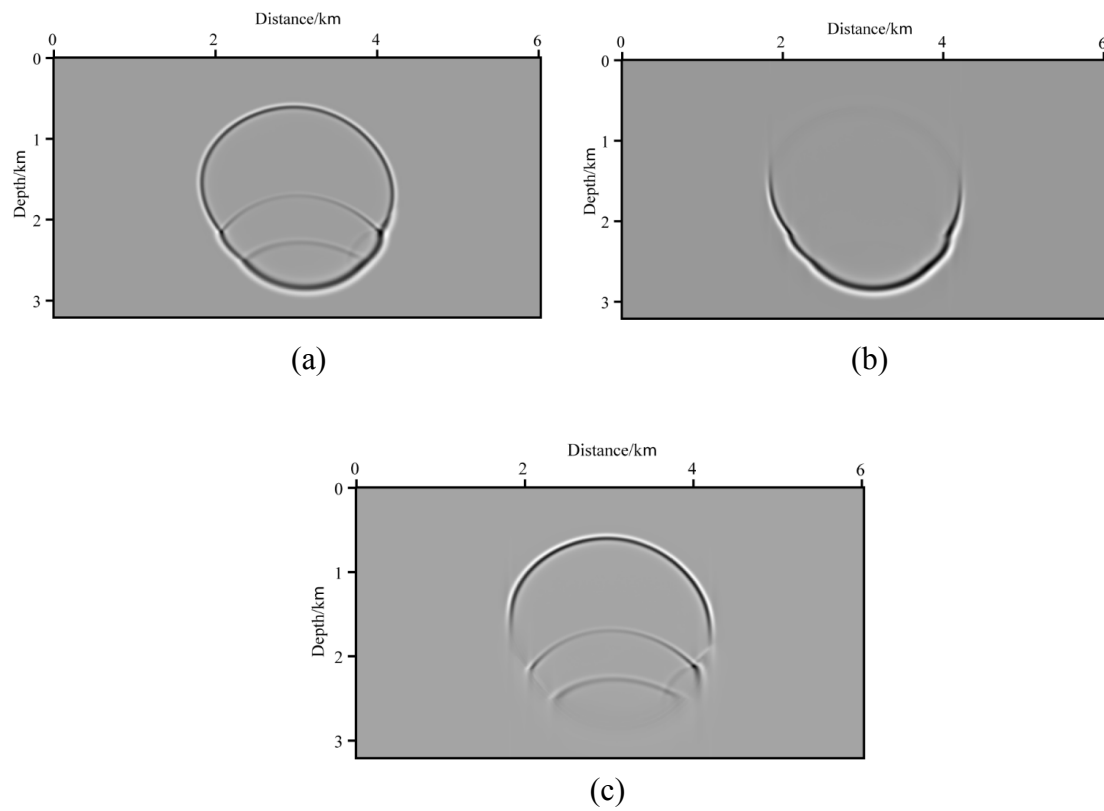
Fig. 4. Decomposed up-going and down-going wavefield for TTI media: (a) full wavefield; (b) down-going wavefield; (c) up-going wavefield

Cross-correlation imaging conditions of wavefield decomposition in TTI media

The cross-correlation imaging conditions of the full wavefields and the decomposed wavefields were tested using a layered-structure model with embedded high seismic-speed salt dunes (Fig. 5). Six surface shots were located between 0 and 6 km. Source interval was 300 m; receivers were evenly distributed on the ground surface. Seismic records had 5000 time steps; time interval was 1 ms.

(a)

(b)

(c)

(d)
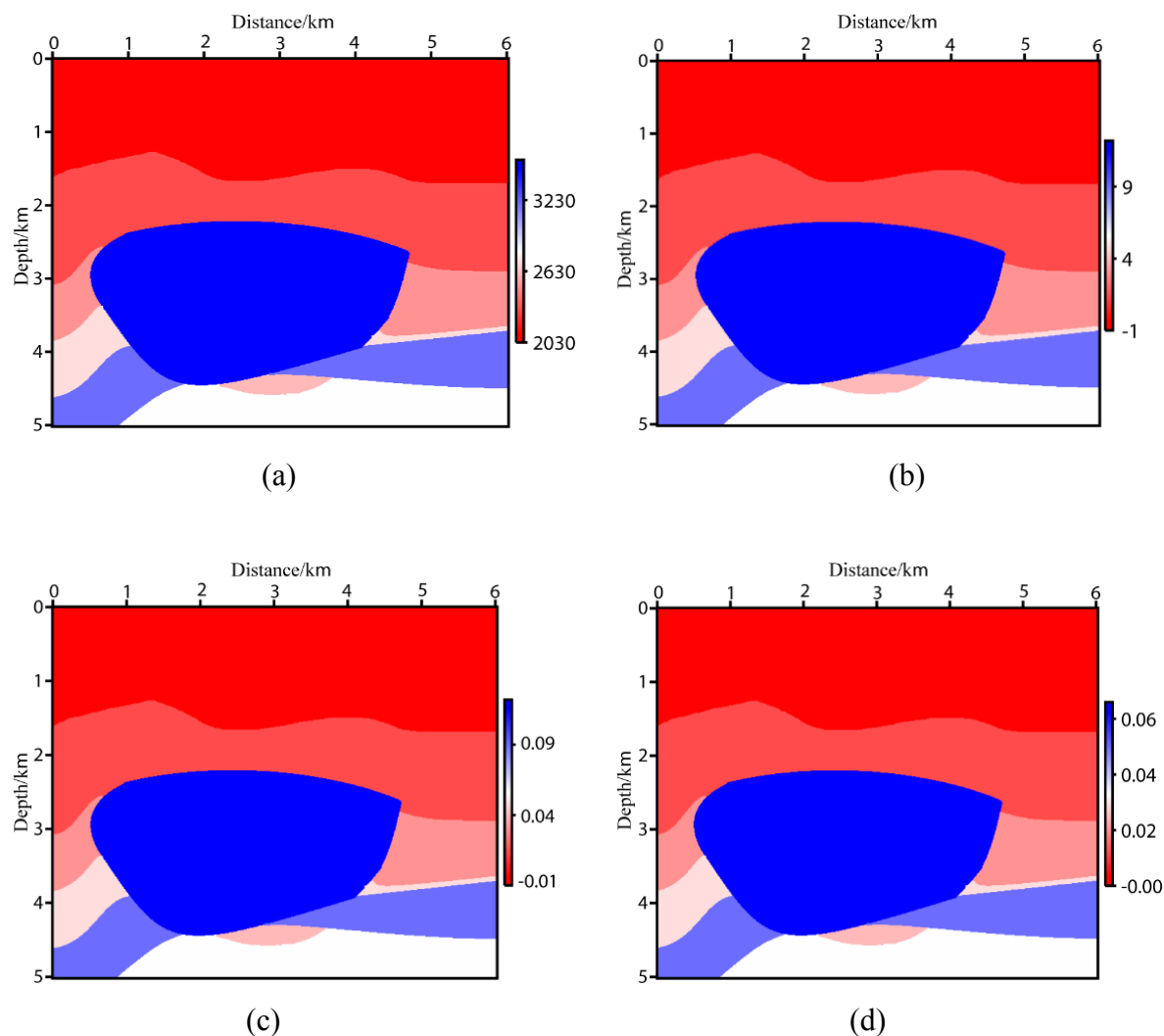
Fig. 5. TTI media model: (a) qP wave velocity along symmetry axis; (b) angle of symmetry axis; (c) ε; (d) δ.

Fig. 6 shows the RTM result obtained for full-wavefield cross-correlation imaging. The large amount of low-frequency noise results from the excessive energy of the low-frequency noise, which has affected the quality of the imaging results.
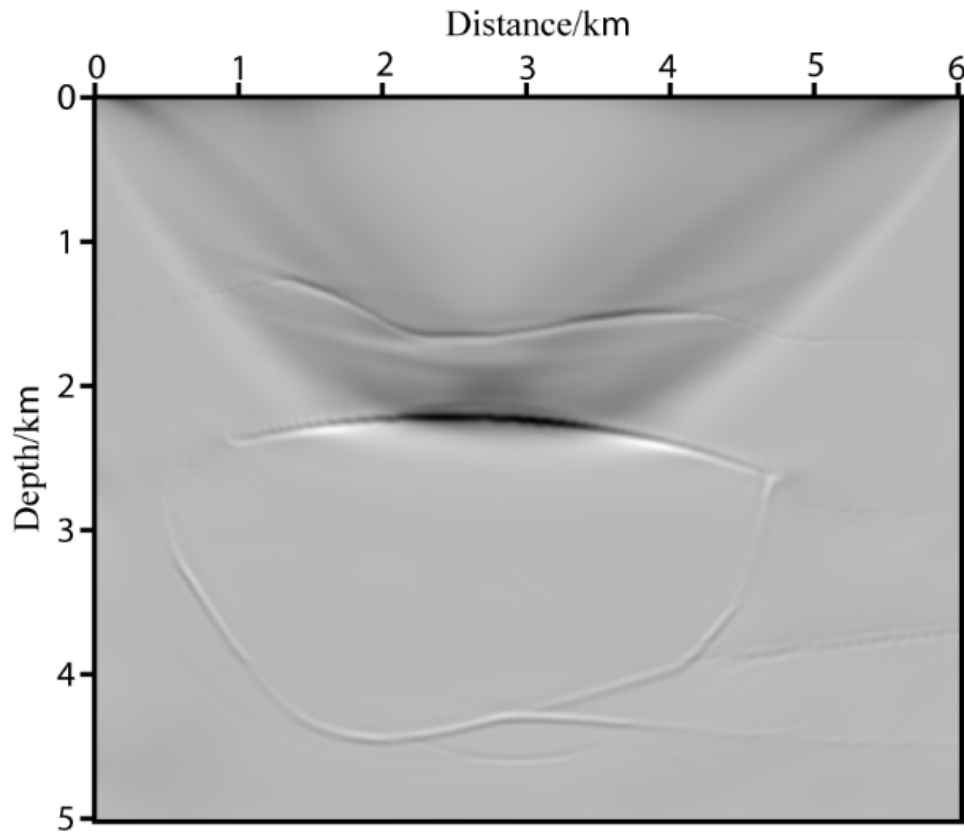
Fig. 6. Reverse-time migration result.

Based on correlation imaging conditions for decomposed seismic wavefields, four results were obtained (Fig. 7) which were not treated for noise suppression. Fig. 7a is the image obtained using the down-going source wavefields and up-going receiver wavefields. This contains the structural information; the other three images, Figs. 7b-d, all show noise interference. It is also very obvious that the signal-to-noise ratio of Fig. 7a is an improvement on Fig. 6.

CONCLUSION

Increasing the anisotropy constraints accurately describes the kinematic characteristics of a seismic wavefield and provides strong support for subsequent RTM. Our study shows that wavefield decomposition of TTI media is achieved using the Hilbert transform. Since RTM imaging artifacts are eliminated by cross-correlation imaging conditions of wavefield decomposition in TTI media, we obtain an image with a high signal-to-noise ratio.
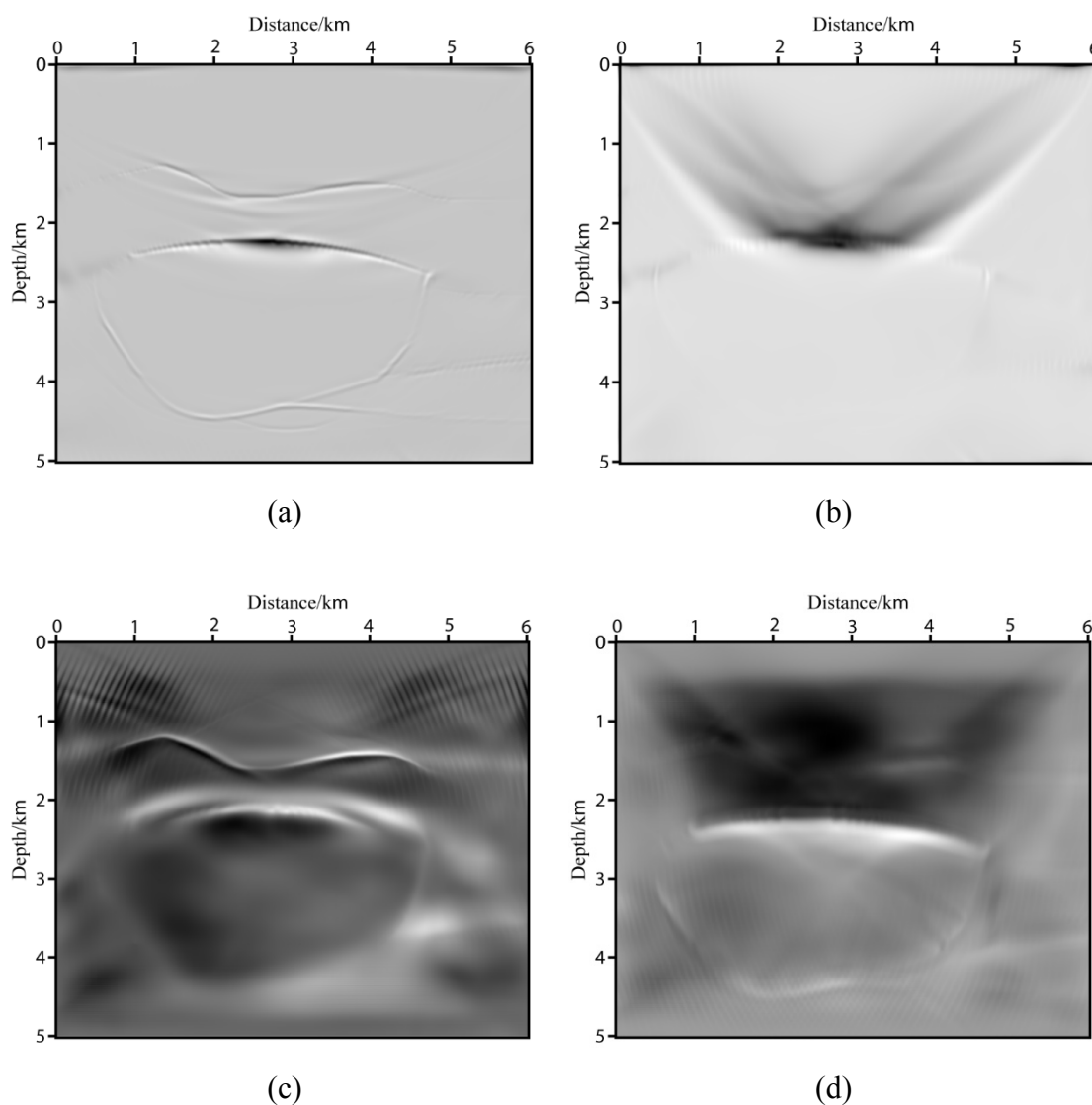
Fig. 7. Reverse-time migration results based on decomposed wavefields: (a) down-going source wave and up-going receiver wave; (b) up-going source wave and down-going receiver wave; (c) up-going source wavefields and up-going receiver wave; (d) down-going source wave and down-going receiver wave.

ACKNOWLEDGMENTS

REFERENCES

Alkhalifah, T., 1998. Acoustic approximations for processing in transversely isotropic media. Geophysics, 2: 623-631.

Duveneck, E. and Bakker, P.M., 2011. Stable P-wave modeling for reverse-time migration in tilted TI media. Geophysics, 76(2): S65-S75.

Fei, T.W., Luo, Y. and Yang, J., 2015. Removing false images in reverse time migration: The concept of de-primary. Geophysics, 80(6): S237-S244.

Fletcher, R.P. and Du, X., 2009. Reverse time migration in tilted transversely isotropic (TTI) media. Geophysics, 74(6): A179-A187.

Liu, H.W., Liu, H., Zhou, Z. and Cui, Y.F., 2010. The problems of denoise and storage in seismic reverse time migration. Chin. J. Geophys., 53: 2171-2180.

Pestana, R.C. and Stoffa, P.L., 2010. Time evolution of the wave equation using rapid expansion method. Geophysics, 75(4): T121-T131.

Pestana, R.C., Ursin, B. and Stoffa, P.L., 2011. Separate P-and SV-wave equations for VTI media. Expanded Abstr., 81st Ann. Internat. SEG Mtg., San Antonio: 163-167.

Shen, P,, Albertin, U. and Corporation, C., 2015. Up-down separation using Hilbert transformed source for causal imaging condition. Expanded Abstr., 85th Ann. Internat. SEG Mtg., New Orleans: 4175-4179.

Sheng, X. and Zhou, H.B., 2014. Accurate simulations of pure quasi-P-waves in complex anisotropic media. Geophysics, 79(6): T341-T348.

Thomsen, L., 1986. Weak elastic anisotropy. Geophysics, 51: 661-672.

Whitmore, N.D., 1983. Iterative depth migration by backward time propagation. Expanded Abstr., 53rd Ann. Internat. SEG Mtg., Las Vegas: 382-385.

Xuan, K, Ying, S. and Weihong, W., 2018. An efficient wavefield simulation and reconstruction method for least-squares reverse time migration. J. Seismic Explor., 27: 183-200.

Xuebao, G., Hong, L., Ying, S. and Weihong, W., 2017. Extracting low-frequency information from time attenuation in elastic waveform inversion. Pure Appl. Geophys., 174: 1303-1314.

Yoon, K. and Marfurt K.J., 2006. Reverse-time migration using the Poynting vector. Geophysics, 37:102-107.

Yoon, K., Suh, S., Ji, J., Cai, J. and Wang, B., 2010. Stability and speedup issues in TTI RTM implementation. Expanded Abstr., 80th Ann. Internat. SEG Mtg., Denver: 3221-3255.

Zhang, Y., Zhang, H.Z. and Zhang, G.Q., 2011. A stable TTI reverse time migration and implementation. Geophysics, 76(3): WA3-WA11.

Zhou, H.B. and Zhang, G.Q., 2006. An anisotropic acoustic wave equation for modeling and migration in 2D TTI media. Expanded Abstr., 76th Ann. Internat. SEG Mtg., New Orleans: 194-198.